

# SUPPORTING INFORMATION

1  
2  
3  
4  
5  
6  
7  
8  
9  
10  
11  
12  
13  
14  
15  
16  
17  
18  
19  
20  
21  
22  
23  
24  
25  
26  
27  
28  
29  
30  
31  
32  
33  
34  
35  
36  
37  
38  
39  
40  
41  
42

## **Understanding the pathways switch of oxygen reduction reaction from single- to double/triple-atom catalysts: dual channel for electron acceptance-backdonation**

Jin Liu<sup>a,#</sup>, Haoxiang Xu<sup>a,#</sup>, Jiqin Zhu<sup>b</sup>, and Daojian Cheng<sup>a,\*</sup>

<sup>a</sup>State Key Laboratory of Organic-Inorganic Composites, Interdisciplinary Research Center for hydrogen energy, Beijing University of Chemical Technology, 100029, Beijing, People's Republic of China

<sup>b</sup>State Key Laboratory of Chemical Resource Engineering, Beijing University of Chemical Technology, 100029, Beijing, People's Republic of China

\*Corresponding authors. [chengdj@mail.buct.edu.cn](mailto:chengdj@mail.buct.edu.cn)

#These authors contribute equally.

## 1 Section 1 Supplementary Method

### 2 S1.1 Gibbs free energy computations

3 The Gibbs free energy ( $G$ ) of the intermediates was calculated by using the  
4 computational hydrogen electrode (CHE) model proposed by Nørskov et al. The  
5 chemical potential of the  $H^+/e^-$  pair in aqueous solution is related to that of half of the  
6  $H_2$  gas molecule at standard hydrogen electrode (SHE) conditions.  $H_2$  at standard  
7 temperature and pressure and  $H_2O$  at its standard vapor pressure were used as references  
8 for H and O, respectively. According to this method, the  $G$  value can be determined as  
9 follows:

$$10 \quad \Delta G = \Delta E - T\Delta S + \Delta E_{ZPE} + \Delta E_{solv}$$

11 where  $\Delta E$  is the reaction energy directly obtained from DFT calculations, and  $T$  is the  
12 temperature ( $T=298.15$  K).  $\Delta E_{ZPE}$  and  $\Delta S$  are the differences between the adsorbed  
13 species and the gas phase molecules in zero-point energy and entropy, respectively.  
14  $E_{solv}$  represents the solvation effects that were simulated by using the Poisson-  
15 Boltzmann continuum-solvation model in the VASPsol code. We take  $pH=0$  in our  
16 calculations for ORR in an acidic electrolyte.

### 18 S1.2 Pre-adsorption phase diagram

19 In this study, we present and discuss the surface preadsorption phase diagram  
20 which allows to analyze the free energy dependence of the various electrochemical  
21 intermediates at varying potential:

$$22 \quad \Delta G = \Delta G_{[U=0,pH=0]} - meU$$

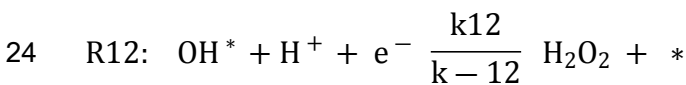
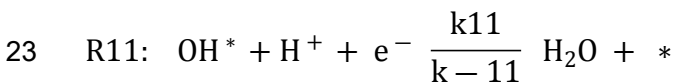
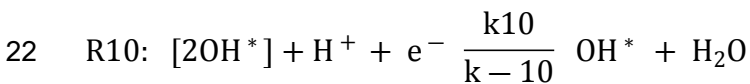
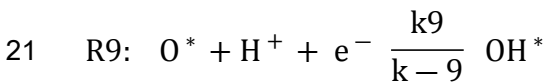
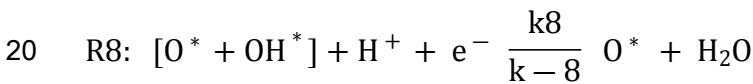
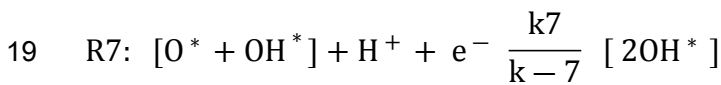
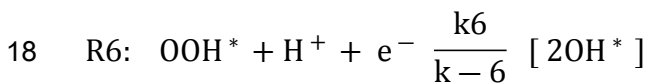
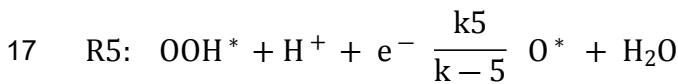
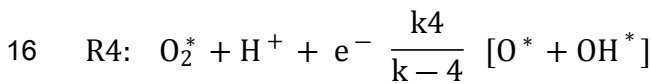
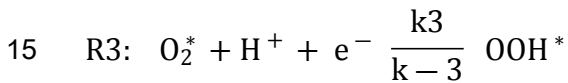
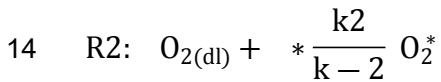
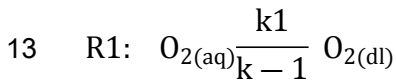
23 The intermediate with the lowest free energy at a given set of potential determines  
24 the stable form of the surface in those conditions. Instead of plotting three-dimensional  
25 graphs, one generally first investigates the dependence with the potential fixing  $pH =$   
26  $0$ . Each intermediate species along the catalytic path for ORR on N-doped graphene is  
27 characterized by a straight line with a negative slope which is determined by the number  
28  $m$  of electrons to be transferred (1 for  $m-G(OH^*)$ , 2 for  $m-G(O^*)$ , and 4 for  $m-G(O_2^*)$ ).

1 In different potential ranges, a different intermediate is found to be the most stable (i.e.,  
 2 the lowest line at a given potential). The resulting surface Pourbaix diagram at T =  
 3 298.15 K and U=0.9V shows clearly which is the most stable form as a function of the  
 4 potential.

5

### 6 **S1.3 Polarization curve simulation.**

7 Following the kinetic model developed by Hansen et al.<sup>1</sup>, we simulated the  
 8 polarization curve of Fe/Co SAC and Fe-Co DACs/TACs. Here, we highlight the  
 9 construction of a complete ORR pathway on Fe-Co DACs/TACs, and electrochemical  
 10 O<sub>2</sub>\* protonation producing O\*+OH\* is identified to be quite thermodynamically and  
 11 kinetically favorable. The O<sub>2</sub> molecule diffusion adsorption, and electrochemical  
 12 reduction steps are listed by the following equations:



25 O<sub>2(aq)</sub> and O<sub>2(dl)</sub> represent O<sub>2</sub> in the electrolyte and the catalyst-electrolyte in interface,

1 respectively. Note that equations R<sub>1</sub> and R<sub>2</sub> are non-electrochemical steps, and the rest  
 2 of equations are electrochemical steps.  $\theta$  represents the coverage of the species. Based  
 3 on the above reduction steps, we can gained the rate equations of each species, such as,

$$4 \quad \frac{\partial \chi_{O_2(dl)}}{\partial t} = k_1 \chi_{O_2(aq)} - k_{-1} \chi_{O_2(dl)} - k_2 \chi_{O_2(dl)} \theta^* + k_{-2} \theta_{O_2^*}$$

$$5 \quad \frac{\partial \theta_{O_2^*}}{\partial t} = k_2 \chi_{O_2(dl)} \theta^* - k_{-2} \theta_{O_2^*} - k_3 \theta_{O_2^*} + k_{-3} \theta_{OOH^*} - k_7 \theta_{O_2^*} - k_{-7} \theta_{[O^* + OH^*]}$$

6 In these equations  $\chi_{H_2O} = 1$  and  $\chi_{O_2(aq)} = 2.34 \cdot 10^{-5}$  corresponding to 1 atm O<sub>2</sub>(g) in  
 7 equilibrium with O<sub>2</sub>(aq). Additionally, site conservation on the Fe/Co SAC site and Fe-  
 8 Co DACs/TACs sites must be satisfied

$$9 \quad 1 = \theta_{O_2^*} + \theta_{OOH^*} + \theta_{O^*} + \theta_{OH^*} + \theta_* + \theta_{[O^* + OH^*]} + \theta_{[2OH^*]}$$

10 The rate equations are solved numerically at steady state, and further infer the turn over  
 11 frequency(TOF).

12 For non-electronchemical step i, its equilibrium constant (K) can be expressed as:

$$13 \quad K_i = \exp \left( - \frac{\Delta G_i}{k_B T} \right)$$

14 where  $\Delta G_i$  is the free energy change of step i, and  $k_B$  is the Boltzmann constant. The  
 15 rate constant ( $k_i$ ) is given by:

$$16 \quad k_i = \frac{k_B T}{h} \exp \left( - \frac{E_{a,i}}{k_B T} \right)$$

17 where  $E_{a,i}$  is the activation energy.

18 While for electrochemical step,  $K_i$  is associated with the reaction potential (U vs RHE),  
 19 given by:

$$20 \quad K_i = \exp \left( - \frac{e(U - U_i)}{k_B T} \right)$$

21 where  $U_i$  is the reversible potential of step i deduced by  $U_i = -G_i/e$ . And the  $k_i$  is written  
 22 as:

$$23 \quad k_i = \frac{k_B T}{h} \exp \left( - \frac{E_{a,i}}{k_B T} \right) \exp \left( - \frac{e\beta_i(U - U_i)}{k_B T} \right)$$

24 where  $\beta_i$  is the symmetric factor taken as 0.5<sup>2</sup>. Since the  $E_{a,i}$  of electrochemical ORR  
 25 steps are generally small range from 0.10 to 0.26 eV<sup>2-4</sup>, we adopted  $E_{a,i} = 0.26$  eV for all  
 26 the electrochemical steps of ORR on Fe/Co SAC and Fe-Co DACs/TACs.

27 Moreover, the rate constants for all the reverse reaction ( $k_i$ ), can be deduced by:

1 
$$k_{-i} = \frac{k_i}{K_i}$$

2 Finally, the current density ( $j$ ) can be calculated by:

3 
$$j = e\alpha n F_0$$

#### 4 **S1.4 Degree of Rate Control**

5 The degree of rate control (DRC) developed by Campbell was used to quantify the  
6 impact of the free energy perturbation  $\delta G_i$  of a specific species  $i$  on the total reaction  
7 rate, which has been widely adopted to identify the rate-controlling transition states (TS)  
8 and intermediates. We slightly modify the original DRC equation to express the impact  
9 of the reaction energy changes on the total reaction rate. The  $DRC_r$  is defined as

10 
$$DRC_{r,n} = \left( \frac{\partial \ln r}{\partial \left( -\frac{G_n}{k_B T} \right)} \right)_{G_m \neq n, G_i^{TS}}$$

11 where  $G_n$  is the reaction energy and  $G_i^{TS}$  is the free energy of a transition state. It  
12 describes the sensitivity of the total reaction rate to the reaction energy.

#### 13 **S1.5 Electronic Structure Analysis**

14 The valance state of Fe-site was investigated by Bader charge analysis (Figure S15). Here,  
15 we found that the valance states of Fe are linear correlated to Fe site transferred charge (namely,  
16  $\Delta e$ ) by Bader charge analysis, so that we can draw a linear fit curve based on three standard  
17 samples (Fe, FeO and Fe<sub>2</sub>O<sub>3</sub>). After calculating the residual charge ( $Re$ ) of Fe site in Fe<sub>1</sub>Co<sub>1-1</sub>,  
18 Fe<sub>2-1</sub>, Fe<sub>2-2</sub> and Fe<sub>3-1</sub>, we found that their corresponding valance states of Fe site are +2.87,  
19 +2.6, +2.59, and +2.63. The  $\Delta e$  is defined as

20 
$$\Delta e = 8 - Re$$

21 where the valance electron number of an metallic Fe atom is 8 and the residual charge ( $Re$ ) that  
22 is the electric charge of Fe site in the corresponding system.

23 The crystal orbital Hamilton population (COHP) analysis was further calculated to obtain  
24 the bonding and antibonding information of the electron densities, which was performed using  
25 the LOBSTER code<sup>5</sup>. The integrated values of the COHP (ICOHP) are convenient to quantify  
26 bond order and compare bond strength.”

1

2

3

4

5

6

7

8

9

10

11

12

13

14

15

16

17

18

19

20

21

22

23 **Section 2 Supplementary Figures**

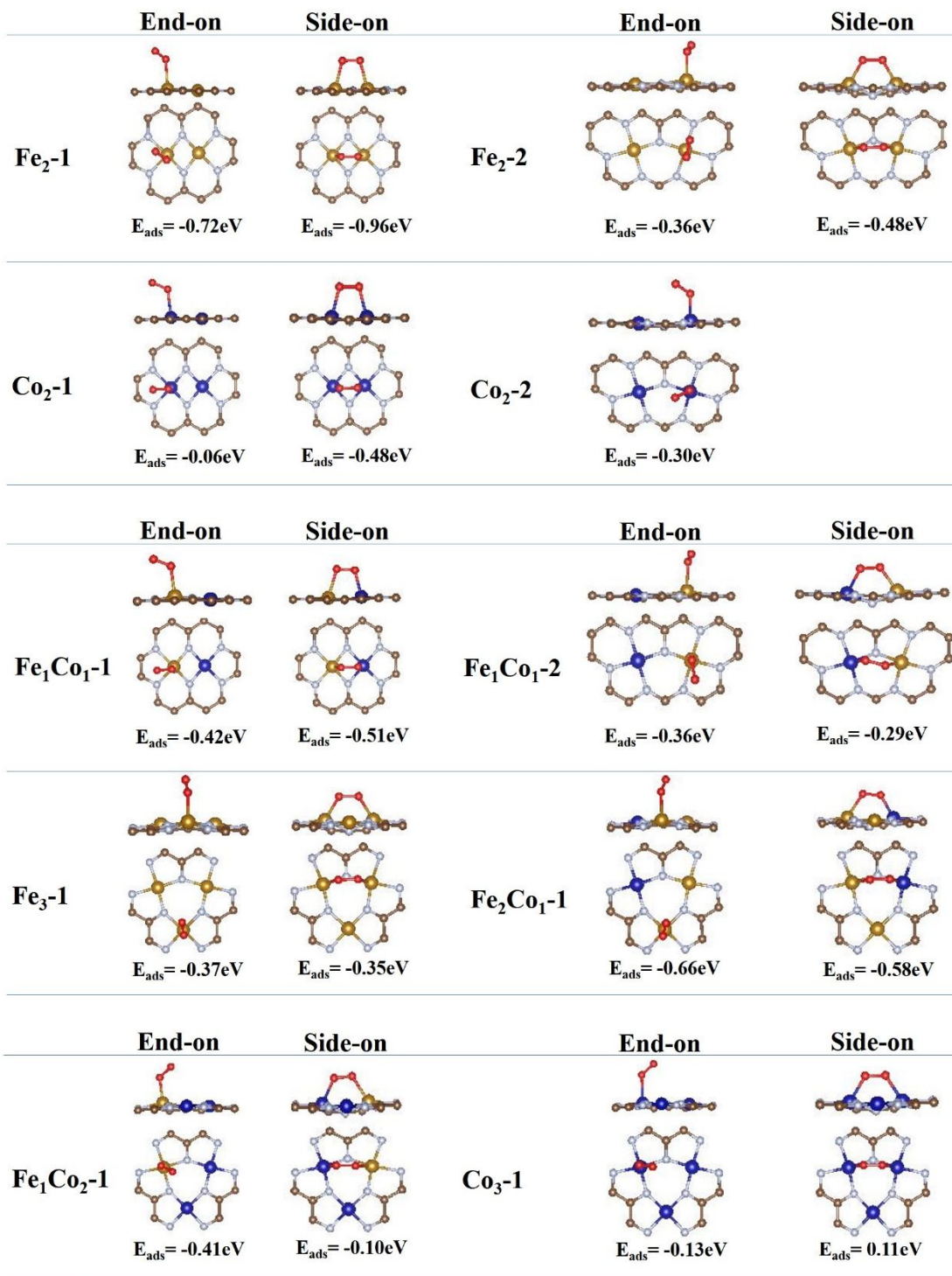
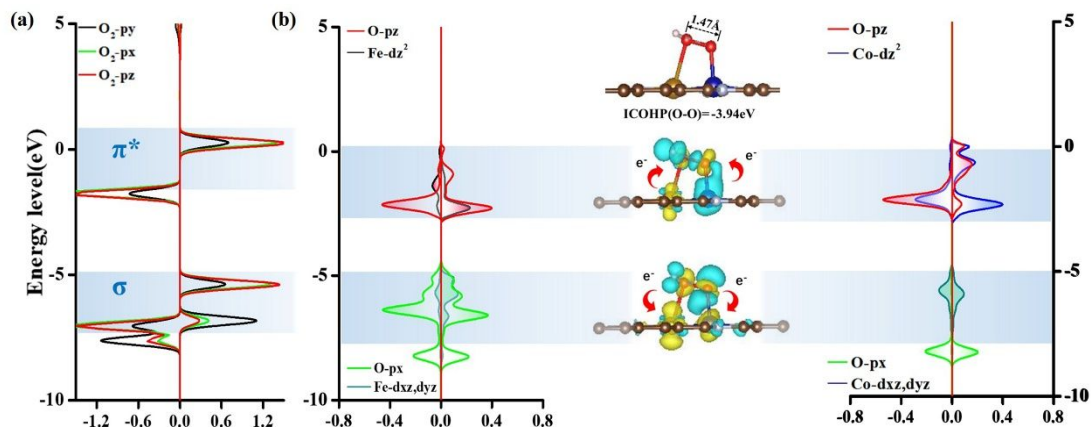
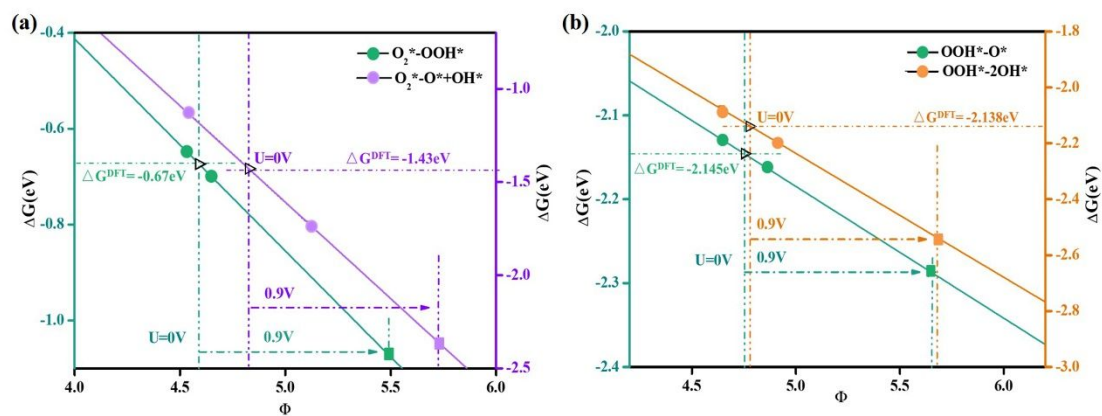


**Figure S1. Adsorption configuration.** The adsorption energy of  $\text{O}_2^*$  with end-on, , and side-on configuration 10  $\text{Fe}_x\text{Co}_{2-x}\text{-NC}/\text{Fe}_x\text{Co}_{3-x}\text{-NC}$  systems.

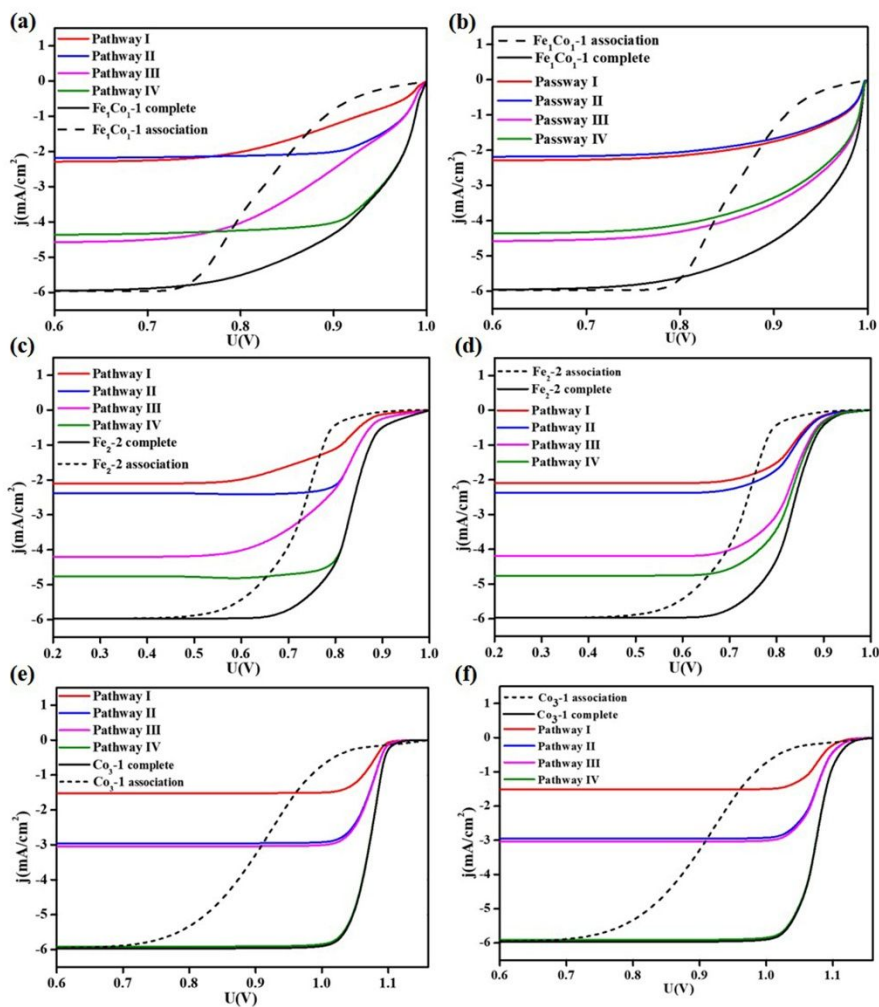


1  
2 **Figure S2.** (a) Partial density of states (PDOS) for O<sub>2</sub>. (b) Partial differential charge density  
3 projecting to specific energy level, projected density of state between OOH and Fe<sub>1</sub>Co<sub>1</sub>-DAC.



5  
6 **Figure S3.** Potential-dependence of the reaction free energy ( $\Delta G$ ) for ORR on Fe-Co DAC to form  
7 (a)  $\Delta G(\text{O}_2^*-\text{OOH}^*)$  and  $\Delta G(\text{O}_2^*-\text{O}^*+\text{OH}^*)$ , (b)  $\Delta G(\text{OOH}^*-\text{O}^*)$  and  $\Delta G(\text{OOH}^*-\text{2OH}^*)$  as  
8 predicted by DFT-PBE. Triangles represent the intersection points of these horizontal lines with  
9 their corresponding  $\Phi$ -dependent reaction free energies within DFT-PBE. The vertical dashed lines  
10 indicate  $\Phi$  associated with applied potentials of 0.0 and 0.9 V as labeled. Squares represent data  
11 extrapolated to an applied potential of 0.9 V.

12  
13  
14  
15



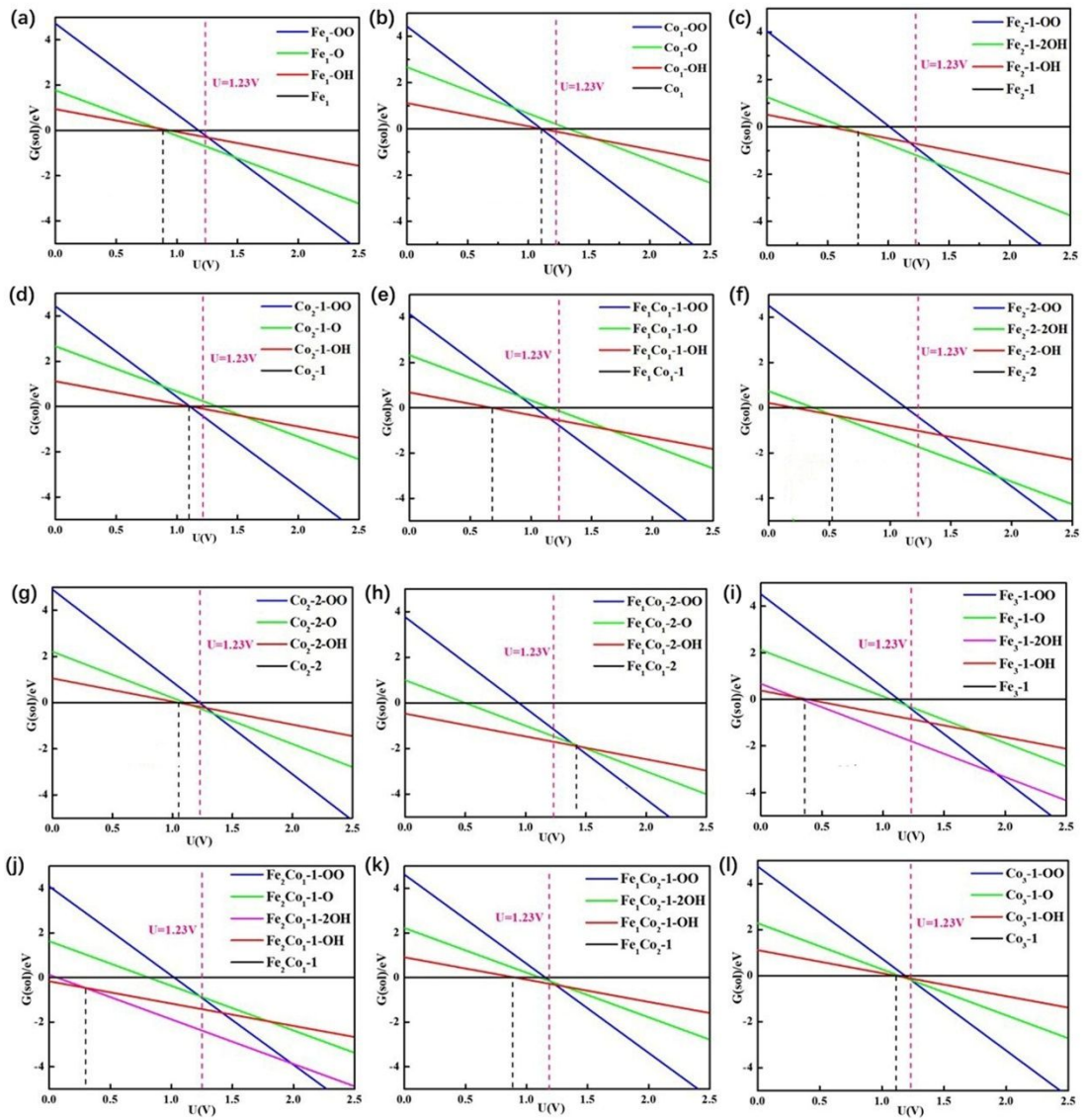
1

2 **Figure S4.** The polarization curves of (a) Fe<sub>1</sub>Co<sub>1</sub>-1 DAC, (c) Fe<sub>2</sub>-2 and (e) Co<sub>3</sub>-1 TAC were  
 3 calculated with an activation energy of 0.26 eV, and polarization curves of (b) Fe<sub>1</sub>Co<sub>1</sub>-1 DAC, (d)  
 4 Fe<sub>2</sub>-2 and (f) Co<sub>3</sub>-1 TAC were calculated with the corresponding O–O bond breaking activation  
 5 barriers.

6

7

8

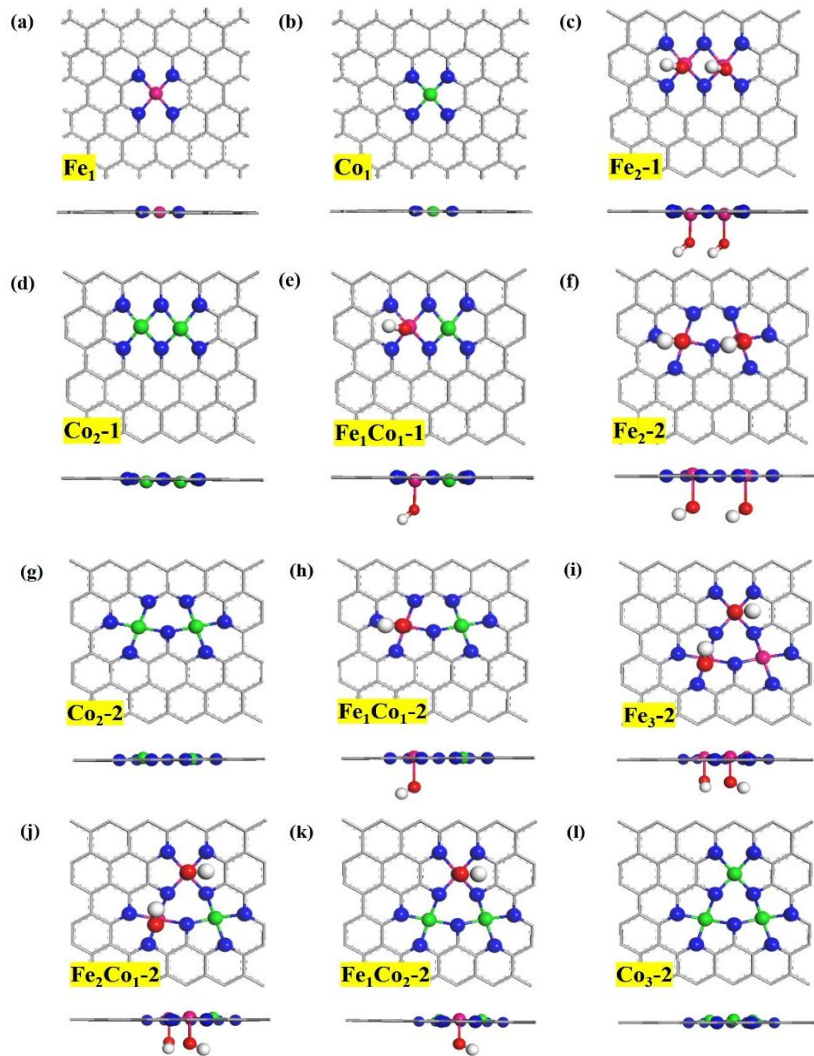


1

2

3 **Figure S5.** Stability of the intermediates of ORR on 10  $\text{Fe}_x\text{Co}_{2-x}\text{NC}/\text{Fe}_x\text{Co}_{3-x}\text{NC}$  systems at pH  
 4 = 0 at varying electrode potential.

5



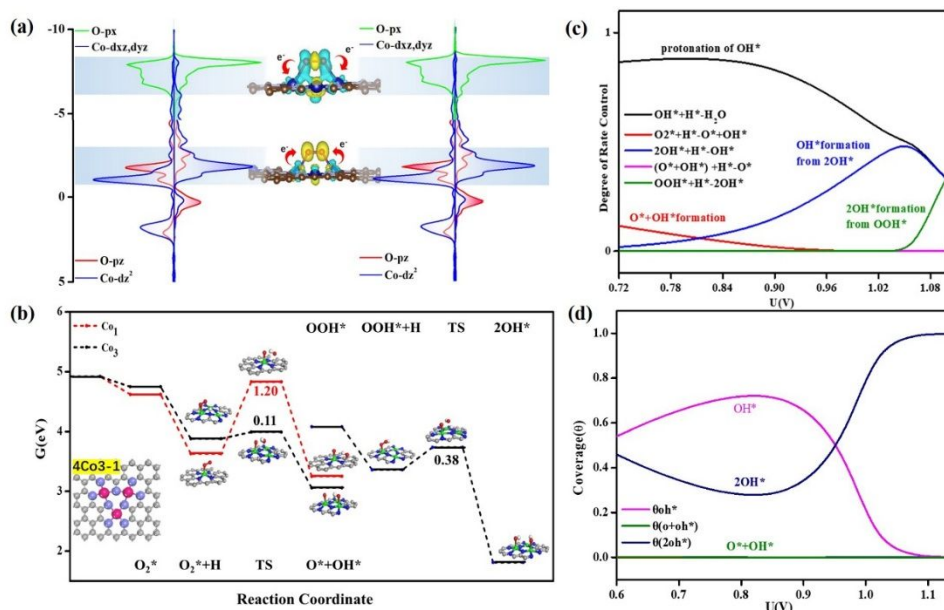
1

2

3 **Figure S6.** The resulting surface pre-adsorption diagram at  $T = 298$  K shows clearly which is the  
 4 most stable form. Color scheme: C, gray; N, blue; pink, Fe; green, Co; red, O; white, H.

5

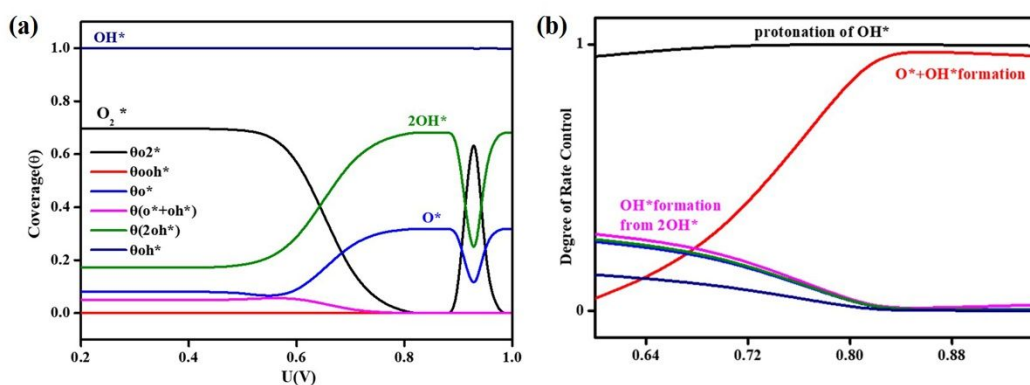
6



1

2 **Figure S7.** (a) Partial differential charge density projecting to specific energy level, projected  
 3 density of state between O<sub>2</sub> on Co<sub>3</sub>-TAC. (b) The O-O bond cleavage barrier of Co-SAC and Co<sub>3</sub>-  
 4 TAC. (c) The coverage and (d) degree of rate control for each elementary step intermediate in  
 5 reaction network as a function of output potential on Co<sub>3</sub>-TAC. Coverage and degree of rate control  
 6 profiles for only the relevant states are shown in the respective panel for each metal, and those not  
 7 explicitly shown indicate zero coverage.

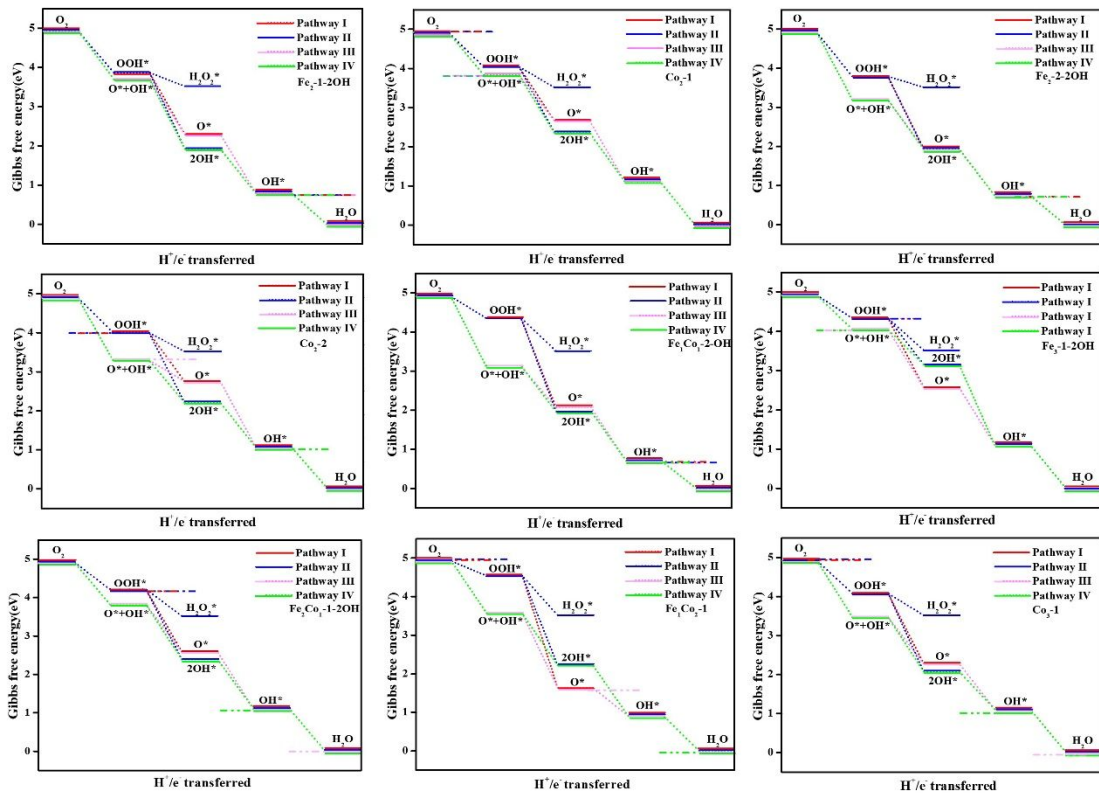
8



9

10 **Figure S8.** (a) The coverage and (b) degree of rate control for each elementary step intermediate in  
 11 reaction network as a function of output potential on Fe<sub>2</sub>-2 DAC. Coverage and degree of rate  
 12 control profiles for only the relevant states are shown in the respective panel for each metal, and  
 13 those not explicitly shown indicate zero coverage. The coverage profiles (except for OH\*) is the  
 14 result of twice uniformization.

1



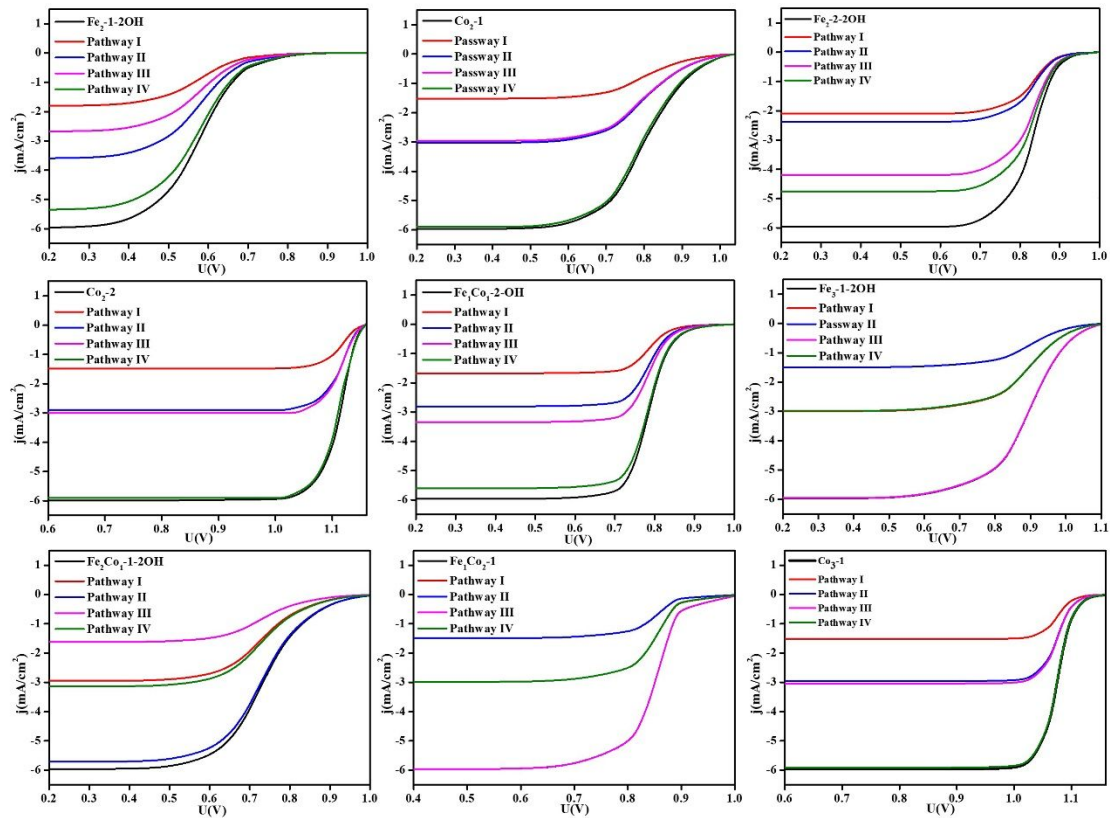
2

3 **Figure S9.** Calculated free energy profiles of complete reaction pathways I-IV for ORR.

4

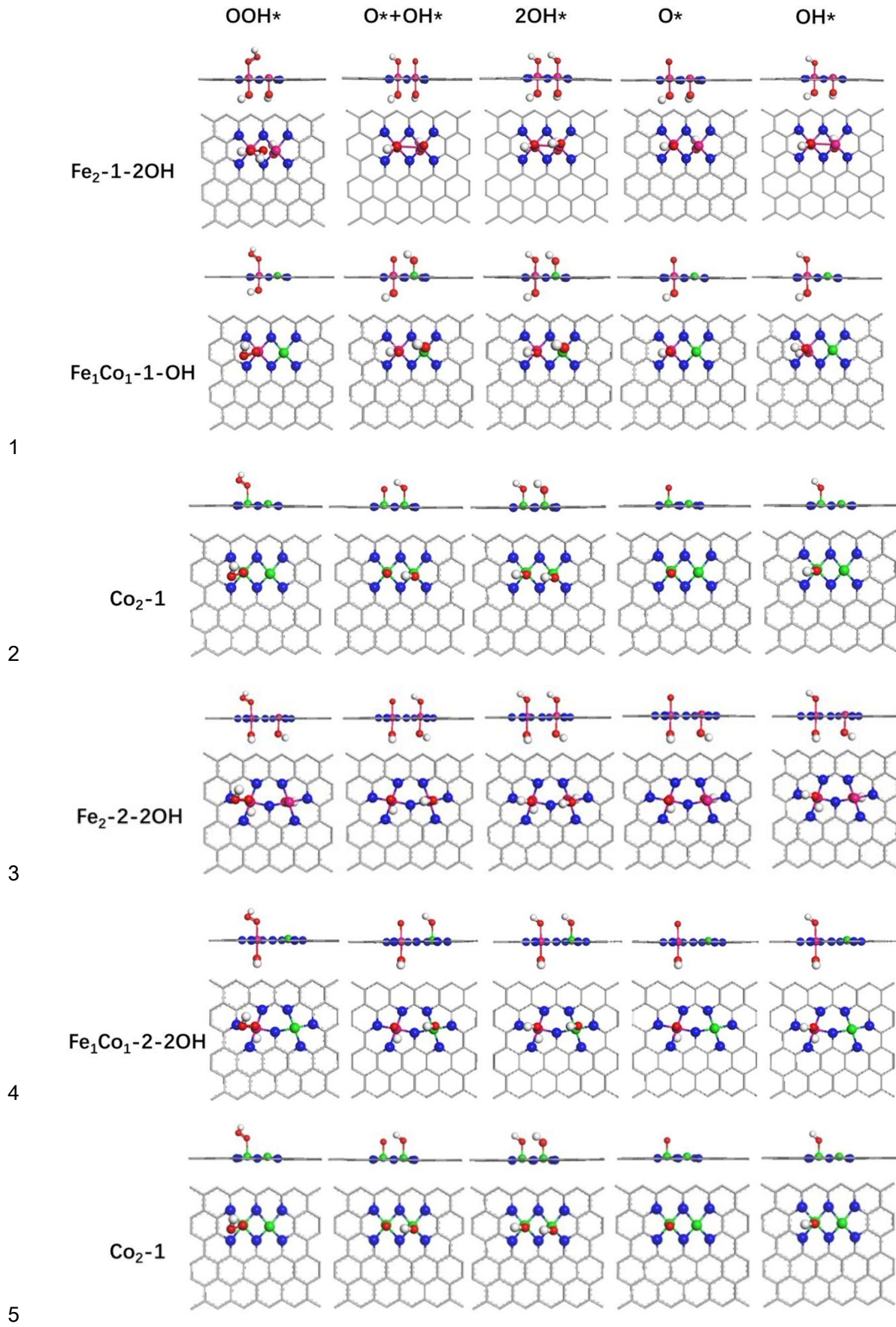
5

6



1  
2  
3  
4  
5  
6  
7  
8

**Figure S10.** Simulated polarization curves of  $\text{Fe}_x\text{Co}_{2-x}\text{-NC}/ \text{Fe}_x\text{Co}_{3-x}\text{-NC}$  systems.



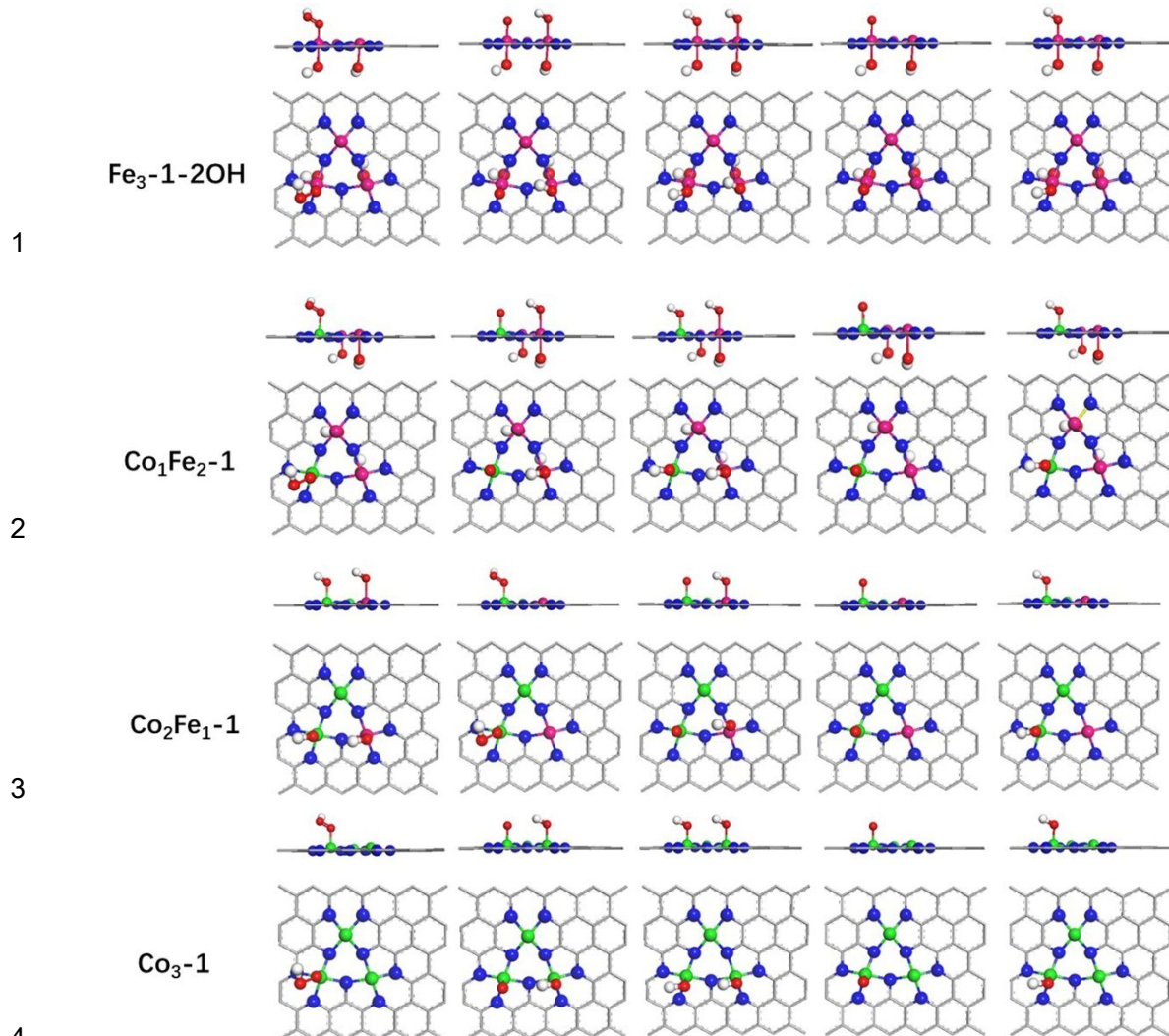
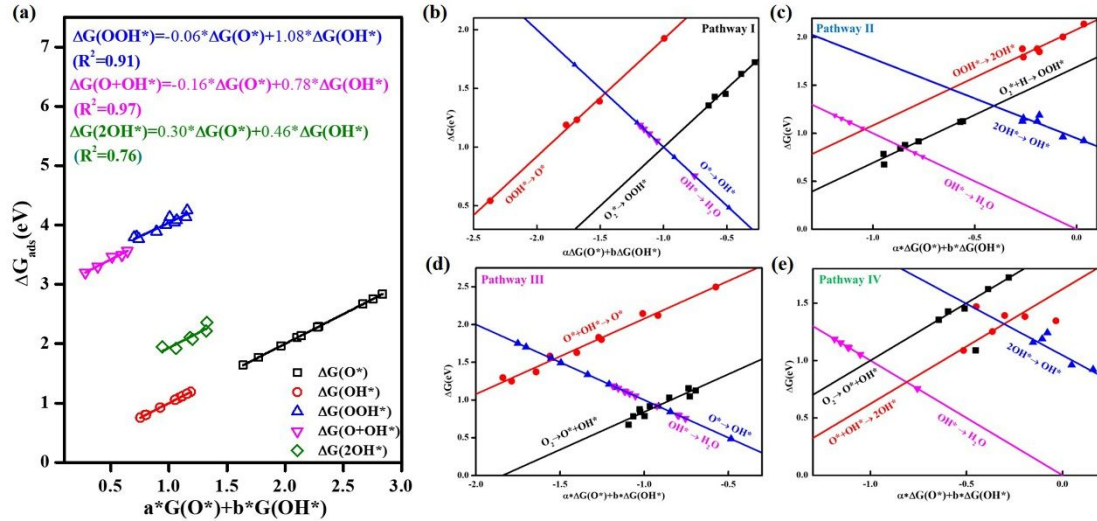
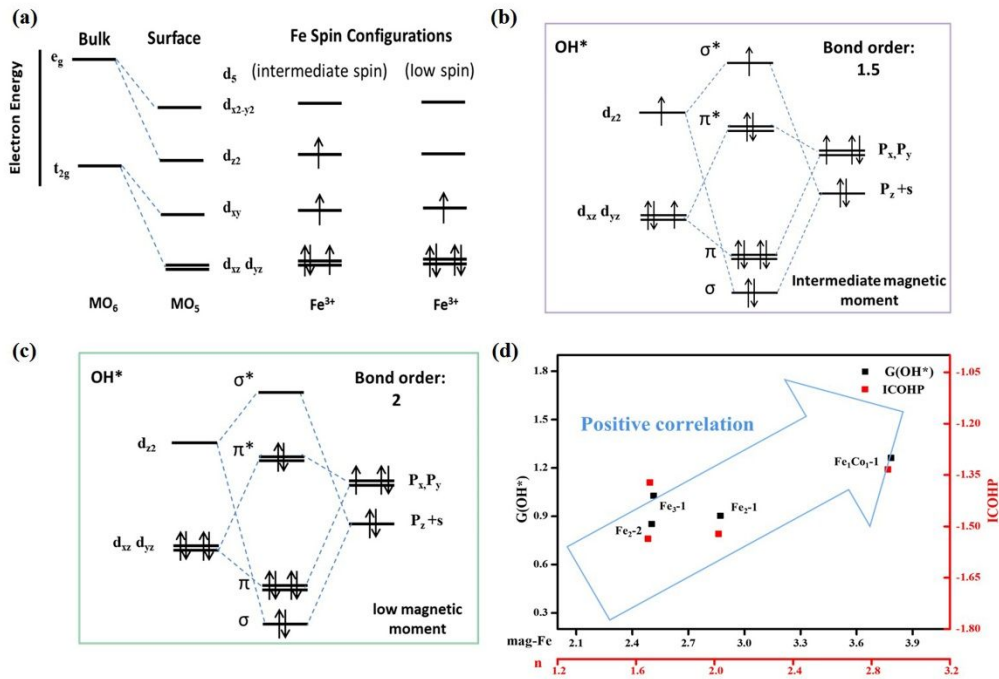


**Figure S11.** Top views of OOH\*, O+OH\*, 2OH\*, O\* and OH\* adsorption on the ten Fe<sub>x</sub>Co<sub>2-x</sub>-NC/  
 Fe<sub>x</sub>Co<sub>3-x</sub>-NC systems. Color scheme: C, gray; N, blue; pink, Fe; green, Co; red, O; white, H.

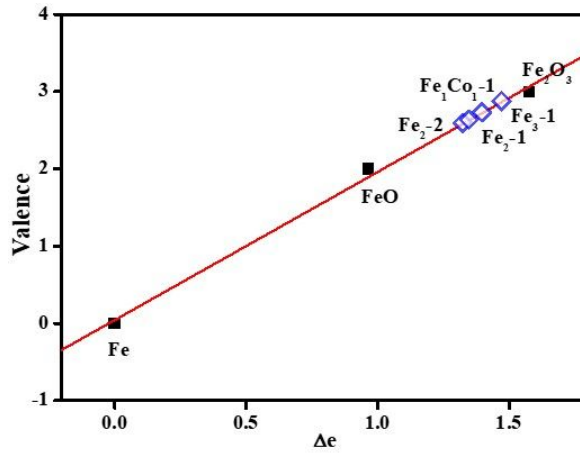


1  
 2 **Figure S12.** (a) Scaling relations between the free energies of OH\*, O\*, 2OH\*, O\*+OH\*, and  
 3 OOH\* on Fe-Co DACs/TACs. (b-e) Scaling relations between free energies changes of each  
 4 elementary step along the four reaction pathways and  $a^* \Delta G(\text{O}^*) + b^* \Delta G(\text{OH}^*)$ . Fit variance of the  
 5 solid lines and a/b in  $a^* \Delta G(\text{O}^*) + b^* \Delta G(\text{OH}^*)$  are shown in Tables S7.  
 6



7  
 8 **Figure S13.** (a) The d-electron configurations of iron cations with intermediate and low spin  
 9 polarization. (b) The orbital interactions between Fe cations with intermediate magnetic moment  
 10 and OH\* intermediate. (c) The orbital interactions between Fe cations with low magnetic moment  
 11 and OH\* intermediate. (d) Linear relationship between  $\Delta G(\text{OH}^*)$  and on-site magnetic moments of  
 12 the Fe center on DACs/TACs (namely, mag-Fe).

1

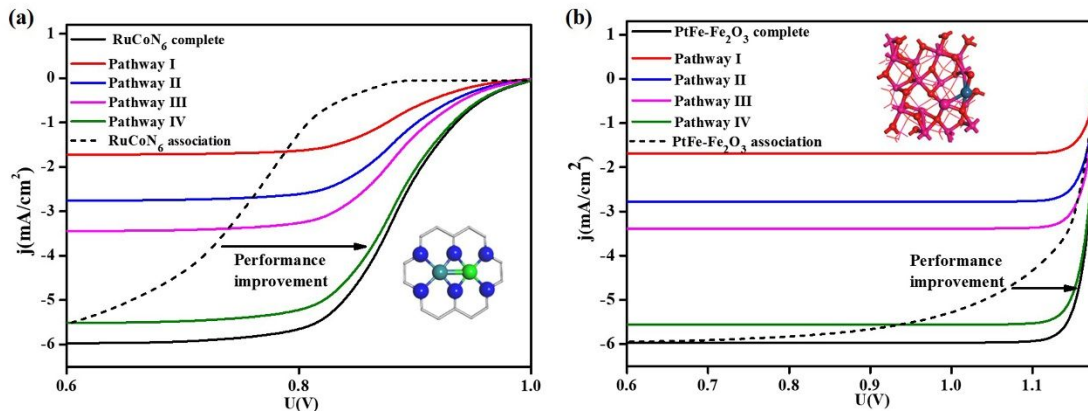


2

3 **Figure S14.** Bader charge analysis reveal Fe site transferred charge (namely,  $\Delta e$ ) in  $\text{Fe}_1\text{Co}_1-1$ ,  $\text{Fe}_2-$   
4  $1$ ,  $\text{Fe}_2-2$  and  $\text{Fe}_3-1$  and linear fitting were carried out to obtain the valence state of Fe atoms in the  
5 corresponding system.

6

7



8

9 **Figure S15.** Simulated polarization curves of ORR on  $\text{RuCo@graphene}$  and  $\text{PtFe@Fe}_2\text{O}_3(012)$ .

10

11

12

13

14

15

1 **Section 3 Supplementary Tables**

2

3 **Table S1.** The dissociation barriers of O-O for different elementary reaction on Fe<sub>1</sub>Co<sub>1</sub>-  
4 1 DAC, Fe<sub>2</sub>-2 DAC and Co<sub>3</sub>-1 TAC with consideration of OH\* preadsorption .

	Fe <sub>1</sub> Co <sub>1</sub> -1 DAC	Fe <sub>2</sub> -2 DAC	Co <sub>3</sub> -1 TAC
O <sub>2</sub> *+H*→	0.56eV	0.83eV	0.11eV
O*+OH*			
OOH*+H*→	0.25eV	0.28eV	0.38eV
2OH*			

5

6 **Table S2.** Half-wave potentials ( $E_{1/2}$ ) and  $E_{\text{onset}}$  for ORR of Fe/Co SAC and Fe-Co  
7 DAC obtained from various simulations and experiments.

$E_{1/2}$ (V vs RHE)	Fe SAC	Co SAC	FeCo DAC	References
Simulations	0.8	0.69	0.96	--
Experiments	0.75	0.75	0.86	6

$E_{\text{onset}}$ ( eV )	Pathway	Fe SAC	Co SAC	FeCo DAC	References
Simulations	I	0.84	0.79	0.67	--
	II	--	--	0.67	
	III	--	--	0.91	
	VI	--	--	0.92	
Experiments	association	0.9	0.88	1.02	7

8

9 **Table S3.** Computed anti-aggregation energy ( $E_{\text{anti-agg}}$ ) and dissolution potential ( $U_{\text{diss}}$ )  
10 are also listed.  
11

Systems	$E_{\text{anti-agg}}$ (eV)	$U_{\text{diss}}$ (V)
Fe <sub>2</sub> -1	-1.45	0.28
FeCo-1	-6.99	3.05
Co <sub>2</sub> -1	-2.48	0.96
Fe <sub>2</sub> -2	-2.75	0.28
FeCo-2	-2.52	0.98
Co <sub>2</sub> -2	-1.82	0.63
Fe <sub>2</sub> -3	0.73	-0.81
FeCo-3	0.18	-0.54
Co <sub>2</sub> -3	-0.82	-0.03
Fe <sub>2</sub> -4	0.57	-0.73

FeCo-4	0.76	-0.83
Co <sub>2</sub> -4	-0.21	-0.18
Fe <sub>2</sub> -5	1.13	-1.01
FeCo-5	0.26	-0.58
Co <sub>2</sub> -5	0.09	-0.32
Co <sub>3</sub> -1	-3.42	1.43
Co <sub>2</sub> Fe <sub>1</sub> -1	-3.36	1.40
Co <sub>1</sub> Fe <sub>2</sub> -1	-2.26	0.68
Fe <sub>3</sub> -1	-2.62	0.86
Co <sub>3</sub> -2	0.56	-0.56
Co <sub>2</sub> Fe <sub>1</sub> -2	1.14	-0.85
Co <sub>1</sub> Fe <sub>2</sub> -2	1.22	-1.06
Fe <sub>3</sub> -2	1.51	-1.20
Co <sub>3</sub> -3	-0.33	-0.11
Co <sub>2</sub> Fe <sub>1</sub> -3	-0.25	-0.15
Co <sub>1</sub> Fe <sub>2</sub> -3	0.53	-0.71
Fe <sub>3</sub> -3	0.26	-0.57
Co <sub>3</sub> -4	5.19	-2.88
Co <sub>2</sub> Fe <sub>1</sub> -4	0.57	-0.56
Co <sub>1</sub> Fe <sub>2</sub> -4	2.17	-1.53
Fe <sub>3</sub> -4	7.23	-4.06
Co <sub>3</sub> -5	1.37	-0.96
Co <sub>2</sub> Fe <sub>1</sub> -5	0.59	-0.58
Co <sub>1</sub> Fe <sub>2</sub> -5	1.09	-0.99
Fe <sub>3</sub> -5	2.21	-1.56

1

2 **Table S4.** Onset potentials ( $E_{\text{onset}}$ ) for ORR of Fe-Co DAC/TAC when considering the  
3 complete pathways and single-site association pathway only, respectively.

<b>Systems</b>	<b>complete pathways</b>	<b>conventional pathway</b>
Fe <sub>2</sub> -1-2OH	0.79eV	0.79eV
Co <sub>2</sub> -1	0.88eV	1.09eV
Fe <sub>1</sub> Co <sub>1</sub> -1-OH	0.67eV	0.92eV
Fe <sub>2</sub> -2-2OH	0.75eV	0.75eV
Co <sub>2</sub> -2	0.92eV	1.05eV
Fe <sub>1</sub> Co <sub>1</sub> -2-OH	0.55eV	0.80eV
Fe <sub>3</sub> -1-2OH	0.58eV	0.87eV
Fe <sub>2</sub> Co <sub>1</sub> -1-2OH	0.71eV	1.09eV
Fe <sub>1</sub> Co <sub>2</sub> -1	0.66eV	1.03eV
Co <sub>3</sub> -1	0.84eV	1.11eV

4

5

6

7

1 **Table S5.** Half-wave potentials ( $E_{1/2}$ ) for ORR of Fe-Co DAC/TAC when considering  
 2 the complete pathways and single-site association pathway only, respectively.

Systems	complete pathways	conventional pathway
Fe <sub>2</sub> -1-2OH	0.6V	0.49V
Co <sub>2</sub> -1	0.82V	1.07V
Fe <sub>1</sub> Co <sub>1</sub> -1-OH	0.93V	0.81V
Fe <sub>2</sub> -2-2OH	0.83V	0.72V
Co <sub>2</sub> -2	1.11V	1.04V
Fe <sub>1</sub> Co <sub>1</sub> -2-OH	0.80V	0.23V
Fe <sub>3</sub> -1-2OH	0.91V	0.61V
Fe <sub>2</sub> Co <sub>1</sub> -1-2OH	0.76V	0.73V
Fe <sub>1</sub> Co <sub>2</sub> -1	0.86V	0.42V
Co <sub>3</sub> -1	1.06V	0.85V

3

4 **Table S6.** Adsorption free energy ( $\Delta G$  in eV) for the ORR intermediates on 10  
 5 Fe<sub>x</sub>Co<sub>2-x</sub>-NC/ Fe<sub>x</sub>Co<sub>3-x</sub>-NC systems in this study.

	OOH*	O*+OH*	O*	2OH*	OH*
Fe <sub>2</sub> -1	3.87	3.80	2.29	1.92	0.79
Fe <sub>1</sub> Co <sub>1</sub> -1	4.25	3.73	2.1	2.11	1.19
Co <sub>2</sub> -1	4.04	3.83	2.67	2.36	1.12
Fe <sub>2</sub> -2	3.79	3.2	1.96	1.94	0.76
Fe <sub>1</sub> Co <sub>1</sub> -2	4.37	3.14	2.07	1.97	0.71
Co <sub>2</sub> -2	4.00	3.3	2.75	2.21	1.05
Fe <sub>3</sub> -1	4.33	4.05	2.57	3.16	1.11
Fe <sub>2</sub> Co <sub>1</sub> -1	4.21	3.82	2.58	2.39	1.10
Fe <sub>1</sub> Co <sub>2</sub> -1	4.54	3.56	1.64	2.22	0.91
Co <sub>3</sub> -1	4.08	3.47	2.28	2.07	1.11

6

7 **Table S7.** Fit variance of the solid lines and a/b in  $a*\Delta G(O^*) + b*\Delta G(OH^*)$  in this  
 8 study.

Pathway I	a	b
O <sub>2</sub> -OOH*	0.00293	-0.92588
OOH*-O*	-1.00293	0.925881
O*-OH*	1	-1
OH*-H <sub>2</sub> O	3.75558E-6	1
Pathway II	a	b
O <sub>2</sub> -OOH*	0.07025	-0.92076
OOH*-2OH*	-0.32853	0.61174
2OH*-OH*	-0.32853	0.61174
OH*-H <sub>2</sub> O	-3.63638E-18	1

Pathway III	a	b
O <sub>2</sub> -O*+OH*	0.15876	-0.78324
O*+OH*-O*	-1.15876	0.78324
O*-OH*	1	-1
OH*-H <sub>2</sub> O	-1.05147E-18	1
Pathway IV	a	b
O <sub>2</sub> -O*+OH*	0.15876	-0.78324
O*+OH*-2OH*	-0.38395	0.5153
2OH*-OH*	0.22733	-0.73456
OH*-H <sub>2</sub> O	-7.2831E-18	1

1

## 2 References

- 3 (1) Hansen, H. A.; Viswanathan, V.; Nørskov, J. K., Unifying Kinetic and  
4 Thermodynamic Analysis of 2 e<sup>-</sup> and 4 e<sup>-</sup> Reduction of Oxygen on Metal Surfaces.  
5 *The Journal of Physical Chemistry C* **2014**, *118* (13), 6706-6718.
- 6 (2) Hansen, H. A.; Varley, J. B.; Peterson, A. A.; Nørskov, J. K., Understanding  
7 Trends in the Electrocatalytic Activity of Metals and Enzymes for CO<sub>2</sub> Reduction to  
8 CO. *J Phys Chem Lett* **2013**, *4* (3), 388-92.
- 9 (3) Tripković, V.; Skúlason, E.; Siahrostami, S.; Nørskov, J. K.; Rossmeisl, J.,  
10 The oxygen reduction reaction mechanism on Pt(111) from density functional theory  
11 calculations. *Electrochimica Acta* **2010**, *55* (27), 7975-7981.
- 12 (4) Jinnouchi, R.; Kodama, K.; Hatanaka, T.; Morimoto, Y., First principles based  
13 mean field model for oxygen reduction reaction. *Phys Chem Chem Phys* **2011**, *13* (47),  
14 21070-83.
- 15 (5) Maintz, S.; Deringer, V. L.; Tchougreff, A. L.; Dronskowski, R., LOBSTER:  
16 A tool to extract chemical bonding from plane-wave based DFT. *J Comput Chem* **2016**,  
17 *37* (11), 1030-5.
- 18 (6) Wang, J.; Huang, Z.; Liu, W.; Chang, C.; Tang, H.; Li, Z.; Chen, W.;  
19 Jia, C.; Yao, T.; Wei, S.; Wu, Y.; Li, Y., Design of N-Coordinated Dual-Metal  
20 Sites: A Stable and Active Pt-Free Catalyst for Acidic Oxygen Reduction Reaction. *J*  
21 *Am Chem Soc* **2017**, *139* (48), 17281-17284.
- 22 (7) Xiao, M.; Chen, Y.; Zhu, J.; Zhang, H.; Zhao, X.; Gao, L.; Wang, X.;  
23 Zhao, J.; Ge, J.; Jiang, Z.; Chen, S.; Liu, C.; Xing, W., Climbing the Apex of  
24 the ORR Volcano Plot via Binuclear Site Construction: Electronic and Geometric  
25 Engineering. *J Am Chem Soc* **2019**, *141* (44), 17763-17770.

26